The Journal of Experimental Biology 212, 2149-2158
Published by The Company of Biologists 2009
doi:10.1242/jeb.029868

Lift and drag performance of odontocete cetacean flippers

Paul W. Weber[1], Laurens E. Howle[1,2,*], Mark M. Murray[3] and Frank E. Fish[4]

[1]Mechanical Engineering and Materials Science Department and [2]Center for Nonlinear and Complex Systems, Duke University, Durham, NC 27708, USA, [3]Mechanical Engineering Department, United States Naval Academy, Annapolis, MD 21402, USA and [4]Department of Biology, West Chester University, West Chester, PA 19383, USA

*Author for correspondence (e-mail: laurens.howle@duke.edu)

Accepted 11 April 2009

SUMMARY

Cetaceans (whales, dolphins and porpoises) have evolved flippers that aid in effective locomotion through their aquatic environments. Differing evolutionary pressures upon cetaceans, including hunting and feeding requirements, and other factors such as animal mass and size have resulted in flippers that are unique among each species. Cetacean flippers may be viewed as being analogous to modern engineered hydrofoils, which have hydrodynamic properties such as lift coefficient, drag coefficient and associated efficiency. Field observations and the collection of biological samples have resulted in flipper geometry being known for most cetacean species. However, the hydrodynamic properties of cetacean flippers have not been rigorously examined and thus their performance properties are unknown. By conducting water tunnel testing using scale models of cetacean flippers derived *via* computed tomography (CT) scans, as well as computational fluid dynamic (CFD) simulations, we present a baseline work to describe the hydrodynamic properties of several cetacean flippers. We found that flippers of similar planform shape had similar hydrodynamic performance properties. Furthermore, one group of flippers of planform shape similar to modern swept wings was found to have lift coefficients that increased with angle of attack nonlinearly, which was caused by the onset of vortex-dominated lift. Drag coefficient *versus* angle of attack curves were found to be less dependent on planform shape. Our work represents a step towards the understanding of the association between performance, ecology, morphology and fluid mechanics based on the three-dimensional geometry of cetacean flippers.

Key words: cetacean, drag, lift, odontocete, flipper, hydrodynamics, computed tomography.

INTRODUCTION

For all species of aquatic vertebrates, swimming performance depends upon the animal's control surfaces, which include flippers, flukes and fins. Flippers are one of the principal control surfaces of cetaceans (whales, dolphins and porpoises) due to their position (i.e. anterior of the center of mass) and mobility (i.e. three degrees of freedom). The flippers assist in stabilizing the body during swimming and contribute to a variety of underwater maneuvers, including braking, diving, lateral turning, rolling, paddling and surfacing (Fish, 2000; Fish, 2002; Fish and Battle, 2005; Fish and Lauder, 2006; Woodward et al., 2006; Cooper et al., 2008). Flippers are modifications of the pectoral limbs of terrestrial animals, which evolved for aquatic use after cetaceans moved from the terrestrial to the aquatic environment in the Eocene epoch (Thewissen, 1998; Fish, 2004; Cooper et al., 2008).

The cross-section of a typical flipper is similar to that of a modern engineered air/hydrofoil (Fish, 2004; Miklosovic et al., 2004; Johari et al., 2007; Cooper et al., 2008), with a generally rounded leading edge and a sharp trailing edge. Cetacean flippers occur in a wide variety of shapes (hereafter referred to as planforms), from the long, tapering tip planform of the humpback whale (*Megaptera novaeangliae*) flipper to the short, rounded, paddle-like planform of the killer whale (*Orcinus orca*) flipper. The variation in morphology of flippers is associated with the ecology of the cetaceans (Fish and Battle, 2005; Woodward et al., 2006; Cooper et al., 2008).

Cetacean flipper planforms are well catalogued *via* field observations and through biological samples obtained from deceased animals. However, few studies have analyzed the hydrodynamic characteristics of cetacean flippers. Miklosovic et al. tested a model of an idealized flipper of a humpback whale in a wind tunnel and determined the lift, drag and stall characteristics (Miklosovic et al., 2004). Their results indicated that the model emulating the humpback whale flipper geometry with prominent leading edge tubercles displayed superior aerodynamic performance compared with a baseline model with similar planform and cross-sectional geometry but without tubercles. Cooper et al. tested the hydrodynamic performance for a model created from a cast of a minke whale (*Balaenoptera acutorostrata*) flipper (Cooper et al., 2008). The flipper of the minke whale was shown to generate sufficient lift and torque to stabilize the body during maneuvers associated with baleen whale engulfment feeding.

A comparative study of exact replicas of the flippers of different cetacean species has yet to be performed in a controlled environment to determine basic steady hydrodynamic characteristics. The purpose of our study was to measure the hydrodynamic characteristics of a diverse assemblage of flippers from odontocete cetaceans with different ecologies. A major goal of this work was to use three-dimensional models of cetacean flippers as close in geometry to the animal as possible.

MATERIALS AND METHODS

The flippers from seven cetacean species (*Inia geoffrensis* de Blainville, *Stenella coeruleoalba* Meyen, *Phocoena phocoena* Linnaeus, *Lagenorhynchus acutus* Gray, *Tursiops truncates* Montagu, *Kogia breviceps* de Blainville and *Delphinus delphis* Linnaeus) were obtained from dead stranded animals collected by the New Jersey Marine Mammal Stranding Center (Brigantine, NJ,

USA) or in the marine mammal alcoholic collection of the Natural History Museum of the Smithsonian Institution (Washington, DC, USA). Animals collected by the stranding center were transported to the University of Pennsylvania School of Veterinary Medicine, New Bolton Center for necropsy. Flippers were removed from the carcass, sealed in plastic bags and subsequently frozen at –19°C and stored at West Chester University. These flippers remained frozen as they were transported to the Woods Hole Oceanographic Institution (WHOI, Woods Hole, MA, USA) for CT (computed tomography) scanning. Prior to scanning the flippers were allowed to thaw. Eleven different specimens from seven different cetacean species (Tables 1 and 2) were chosen for this work.

CT scans were obtained with a Siemens Volume Zoom or Siemens Somaton Emotion CT scanner (Siemens Medical Solutions USA, Malvern, PA, USA) at the Woods Hole Oceanographic Institution Ocean Imaging Center and with Siemens Somaton SP scanner (Siemens Medical Solutions USA) located in the Department of Anthropology of the Natural History Museum of the Smithsonian Institution. The details for CT scanning have been provided in papers by Marino et al. (Marino et al., 2003) and Fish et al. (Fish et al., 2007). CT data were acquired for the entire span of flipper (i.e. distance from anterior insertion of flipper with body to the distal tip) at 100 μm slice intervals. All images were provided as 512×512 matrix DICOM (Digital Imaging and Communications in Medicine format) outputs.

A custom-written program in C#.NET (Microsoft Corporation, Redmond, WA, USA) was used to render the CT output into a file that could be read by a computer-aided design package (SolidWorks 2007, Dassault Systèmes SolidWorks, Concord, MA, USA). The flipper models were scaled to within the limitations of the water tunnel, which required that the models be no more than 20.3 cm in height and 25.4 cm in length to minimize wall effects and tunnel blockage. Scaling was also necessary because exact unscaled replicas of some cetacean flippers tested would have resulted in models that were either too large to fit into the tunnel or too small to yield reliable measurements with the equipment used. A three-dimensional rapid prototype machine (3D Systems SinterStation HiQ Series SLS System, 3D Systems, Rock Hill, SC, USA) was used to construct the flipper models. Our studies were limited to rigid, non-flexible flippers in steady flow and we did not consider flipper motion. Fig. 1 gives an overview of the stages of the model construction process. The planform shapes of all eleven models tested are shown in Fig. 2.

Experiments were conducted in the closed-circuit water tunnel facility at the United States Naval Academy (USNA, Annapolis, MD, USA) Hydromechanics Laboratory. This recirculating tunnel consists of a 0.4 m×0.4 m square test section that is 1.8 m in length and is capable of speeds of over 6 m s^{-1}. The tunnel features flow management devices, including turning vanes in the tunnel corners and a honeycomb flow straightener in the settling chamber. The turbulence intensity in the tunnel is approximately 0.5%. Further details of the water tunnel may be found in Schultz and Flack (Schultz and Flack, 2003).

The flipper models were mounted in the water tunnel with a custom-designed experimental apparatus, which held the models in a known orientation and allowed for changes in the angle of attack (α; incident angle of water flow to chord of model) from –90 deg. to 90 deg. (although testing rarely required exceeding 50 deg. in either direction). The load cell, which was used for measurement of flipper forces (lift and drag) and moments, was an Advanced

Table 1. Select hydrodynamic performance parameters for the cetacean flipper models tested (*Re*=250,000 match trials)

Common name (scientific name) (catalogue number)	$C_{L,max}$	$\alpha_{C_{L,max}}$ (deg.)	$C_{D,min}$	$\alpha_{C_{D,min}}$ (deg.)	Linear portion(s) of C_L curve slope (deg.$^{-1}$)	Planform type
Amazon river dolphin (*Inia geoffrensis*) (001)	1.101	24	0.0477	0	0.0522	Triangular
Striped dolphin (*Stenella coeruleoalba*) (015)	0.907	46	0.0131	8	0.0376 (–13 deg. to 7 deg.), 0.0193 (8 deg. to 19 deg.), 0.0295 (20 deg. to $C_{L,max}$)	Swept pointed
Harbor porpoise (*Phocoena phocoena*) (034)	1.262	22	0.0327	–17	0.0457	Swept pointed
Atlantic white-sided dolphin (*Lagenorhynchus acutus*) (055)	1.139	36	0.0375	–1	0.0397 (–32 deg. to –4 deg.), 0.0198 (–3 deg. to 2 deg.), 0.0370 (3 deg. to $C_{L,max}$)	Swept pointed
Bottlenose dolphin (*Tursiops truncatus*) (056)	1.362	29	0.0397	5	0.0593	Triangular
Pygmy sperm whale (*Kogia breviceps*) (058)	1.076	32	0.0319	–3	0.0616	Triangular
Pygmy sperm whale (*Kogia breviceps*) (059)	0.847	18	0.0428	–3	0.0636	Triangular
Common dolphin (*Delphinus delphis*) (070)	1.055	35	0.0352	–6	0.0378 (–33 deg. to –7 deg.), 0.0139 (–6 deg. to 2 deg.), 0.0370 (3 deg. to $C_{L,max}$)	Swept pointed
Harbor porpoise (*Phocoena phocoena*) (075)	1.253	31	0.0245	–6	0.0451 (–39 deg. to –24 deg.), 0.0341 (–23 deg. to 10 deg.), 0.0455 (11 deg. to $C_{L,max}$)	Swept rounded
Bottlenose dolphin (*Tursiops truncatus*) (111)	1.234	41	0.0204	–4	0.0357 (–33 deg. to –4 deg.), 0.0183 (–3 deg. to 9 deg.), 0.0365 (10 deg. to $C_{L,max}$)	Swept rounded
Harbor porpoise (*Phocoena phocoena*) (115)	1.531	36	0.0162	–5	0.0493 (–33 deg. to –12 deg.), 0.0351 (–11 deg. to 8 deg.), 0.0431 (9 deg. to $C_{L,max}$)	Swept rounded

$C_{L,max}$, maximum lift coefficient; $\alpha_{C_{L,max,}}$ angle of attack at maximum lift coefficient; $C_{D.min,}$ minimum drag coefficient; $\alpha_{C_{D,min,}}$ angle of attack at minimum drag coefficient; C_L, lift coefficient; *Re*, Reynolds number.

Table 2. Select hydrodynamic performance parameters for the cetacean flipper models tested (2 m s^{-1} swim speed match trials)

Common name (scientific name) (catalogue number)	$C_{L,max}$	$\alpha_{C_{L,max}}$ (deg.)	$C_{D,min}$	$\alpha_{C_{D,min}}$ (deg.)	Linear portion(s) of C_L curve slope (deg.$^{-1}$)	Flipper *Re* at testing speed
Amazon river dolphin (*Inia geoffrensis*) (001)	1.124	24	0.0435	0	0.0486	254,000
Striped dolphin (*Stenella coeruleoalba*) (015)	1.020	48	0.0171	13	0.0427 (–20 deg. to 6 deg.), 0.0146 (7 deg. to 21 deg.), 0.0377 (22 deg. to $C_{L,max}$)	331,000
Harbor porpoise (*Phocoena phocoena*) (034)	1.256	22	0.0483	–12	0.0449	193,000
Atlantic white-sided dolphin (*Lagenorhynchus acutus*) (055)	1.139	36	0.0375	–1	0.0397 (–32 deg. to –4 deg.), 0.0198 (–3 deg. to 2 deg.), 0.0370 (3 deg. to $C_{L,max}$)	250,000
Bottlenose dolphin (*Tursiops truncatus*) (056)	1.345	28	0.0397	5	0.0578	234,000
Pygmy sperm whale (*Kogia breviceps*) (058)	1.068	31	0.0331	–2	0.0617	227,000
Pygmy sperm whale (*Kogia breviceps*) (059)	0.762	17	0.0369	–3	0.0651	118,000
Common dolphin (*Delphinus delphis*) (070)	1.032	35	0.0303	–6	0.0373 (–33 deg. to –6 deg.), 0.0161 (–5 deg. to 4 deg.), 0.0365 (5 deg. to $C_{L,max}$)	374,000
Harbor porpoise (*Phocoena phocoena*) (075)	1.188	30	0.0791	–4	0.0409 (–39 deg. to –20 deg.), 0.0302 (–19 deg. to 10 deg.), 0.0410 (11 deg. to $C_{L,max}$)	168,000
Bottlenose dolphin (*Tursiops truncatus*) (111)	1.234	41	0.0204	–4	0.0357 (–33 deg. to –4 deg.), 0.0183 (–3 deg. to 9 deg.), 0.0365 (10 deg. to $C_{L,max}$)	259,000
Harbor porpoise (*Phocoena phocoena*) (115)	1.410	35	0.0456	–6	0.0417 (–30 deg. to –6 deg.), 0.0313 (–5 deg. to 8 deg.), 0.0407 (9 deg. to $C_{L,max}$)	120,000

$C_{L,max}$, maximum lift coefficient; $\alpha_{C_{L,max,}}$ angle of attack at maximum lift coefficient; $C_{D,min,}$ minimum drag coefficient; $\alpha_{C_{D,min,}}$ angle of attack at minimum drag coefficient; C_L, lift coefficient; *Re*, Reynolds number.

Mechanical Technology, Dynamometer Model UDW3-6-1000 (AMTI, Watertown, MA, USA), specifically designed for underwater use. LabVIEW version 8.0 (National Instruments, Austin, TX, USA) was used as the data acquisition system, and a custom-written program in C#.NET was used to post-process the data. The experimental procedure consisted of allowing the water tunnel to stabilize at the testing speed, positioning the flipper model to the desired α, collecting the data at that angle, then manually repositioning the model to the next α. Further details concerning model construction and experimental procedure may be found in Weber (Weber, 2008).

Data are reported in terms of the lift (C_L) and drag (C_D) coefficients:

$$C_{L,D} = \frac{F_{L,D}}{\frac{1}{2}\rho U^2 A}, \quad (1)$$

where ($F_{L,D}$) is the measured lift/drag force (N), ρ is the (incompressible) fluid density (kg m^{-3}), U is the water tunnel speed (m s^{-1}) and A is the planform area of the flipper model (m^2). Dynamic similarity was achieved (Shaughnessy et al., 2005) between the models and actual flippers by matching the Reynolds Number (*Re*):

$$Re = \frac{U\bar{C}}{\nu}, \quad (2)$$

where $\bar{C}$ is the mean aerodynamic chord (m) and v is the kinematic viscosity (m^2 s^{-1}). This *Re* matching ensured flow similarity between the model and the flipper.

Testing for each of the 11 models was conducted at two different water tunnel speeds, which were determined by setting the flipper *Re* equal to 250,000 and by setting the animal swim speed equal to 2 m s^{-1}. Note that when the swim speed of 2 m s^{-1} was matched, the *Re* for the model and the animal were the same, assuring similarity (although the *Re* was usually not 250,000; hence, the water tunnel testing speed was generally different). Eqn 2 was used in different forms (depending on *Re* or speed match) to determine appropriate water tunnel flow speeds given the geometric parameters and water temperatures of both the model and animal.

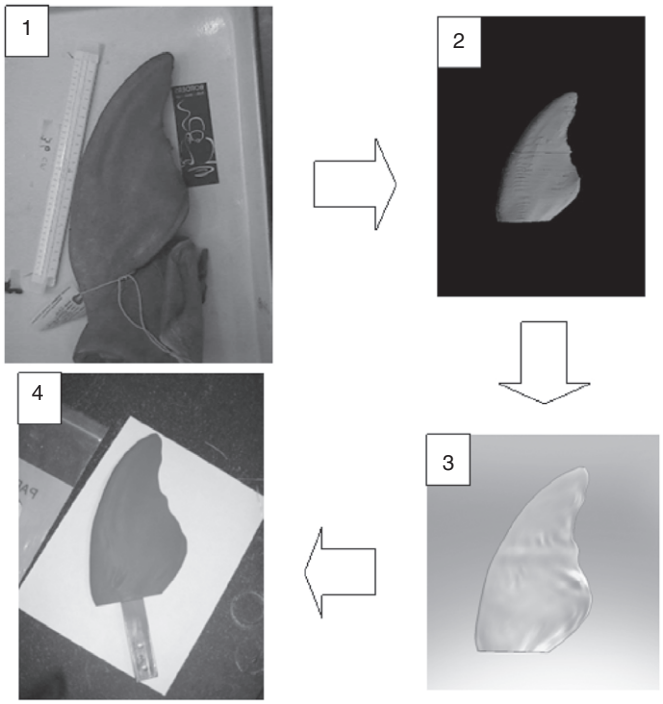

Fig. 1. Three-dimensional scale model construction process. (1) Photograph and computed tomography (CT) scan (not shown) of animal flipper specimen, Amazon River dolphin *Inia geoffrensis* (catalogue number 001). (2) Output from C#.NET CT scan processing program. (3) Computer aided design (CAD) rendering of fin model. (4) Flipper model for water tunnel testing.

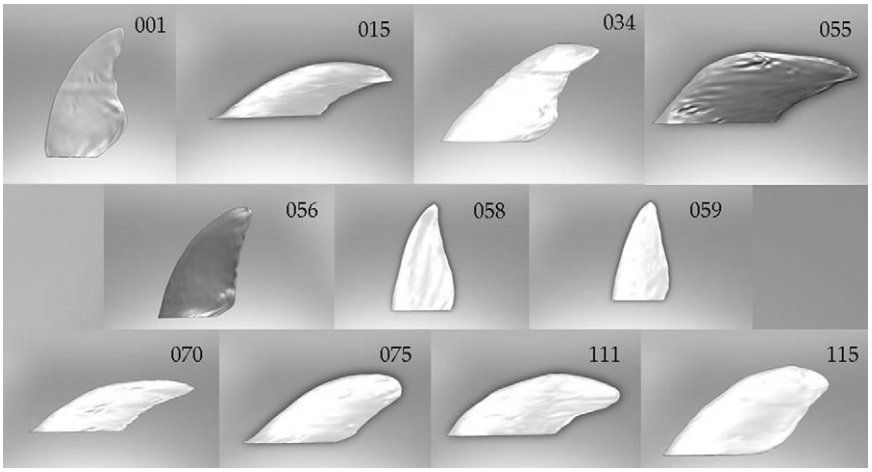

Fig. 2. Computer aided design (CAD) rendering of all fin models tested with catalogue numbers. From top left: *Inia geoffrensis* 001, *Stenella coeruleoalba* 015, *Phocoena phocoena* 034, *Lagenorhynchus acutus* 055, *Tursiops truncatus* 056, *Kogia breviceps* 058, *Kogia breviceps* 059, *Delphinus delphis* 070, *Phocoena phocoena* 075, *Tursiops truncatus* 111, *Phocoena phocoena* 115. Tables 1 and 2 give the common names of these animals.

Re of 250,000 was chosen to minimize boundary layer effects. A test speed of $2\,m\,s^{-1}$ was chosen because field observations and data have confirmed that all animals from which models were made were known to be able to swim at this speed (Fish and Rohr, 1999). Additional factors that led to the choice of 250,000 as the *Re* match and $2\,m\,s^{-1}$ as the swim speed match included limitations of the water tunnel and the load cell and consideration of low-speed fluid dynamic effects. If the *Re* or swim speed match was chosen at a value that was too low, then the load cell would have difficultly resolving the resulting small forces, and low *Re* fluid dynamic effects, such as thick boundary layers and laminar boundary layer detachment and reattachment, would have to be considered. If the *Re* or swim speed match was chosen at a value that was too high, then the speed capabilities of the water tunnel and load capabilities of the load cell could possibly be exceeded.

Experimental error analysis was conducted using standard techniques as outlined in Fox and McDonald (Fox and McDonald, 1999). Sources of error in the experiment included uncertainties in the load cell, uncertainties in the Pitot tube voltage reading, uncertainties in tabulated values of density and kinematic viscosity, uncertainties in the calibration curve for the Pitot tube and uncertainties in geometry due to the model construction process. The error analysis determined how these individual uncertainties propagated into overall uncertainties for quantities that depended upon them (e.g. the uncertainty in the water tunnel speed depended upon the uncertainty of both the Pitot tube voltage reading and the Pitot tube calibration curve). The analysis determined that the maximum uncertainty in the water tunnel speed was ±7%, the maximum uncertainty in the *Re* was ±8% and the maximum uncertainty in C_L and C_D measurements was ±15%.

The specimens tested could be grouped into one of three categories according to their general planform shape: (1) triangular (with no sweep), (2) swept with pointed tip, and (3) swept with rounded tip. The planform shapes for each flipper are listed in Table 1 and shown pictorially in Fig. 2. For statistical comparisons, the animals were grouped according to their mean swim speeds in the wild. The slow group was defined as animals that swim at mean speeds of less than $1.5\,m\,s^{-1}$ and consisted of *I. geoffrensis* and *K. breviceps*. The medium group was defined as animals that swim at mean speeds between $1.5\,m\,s^{-1}$ and $2.8\,m\,s^{-1}$ and consisted of *T. truncatus* and *P. phocoena*. The fast group was defined as animals that swim at mean speeds greater than $2.8\,m\,s^{-1}$ and consisted of *D. delphis, L. acutus* and *S. coeruleoalba*.

RESULTS

The experimental data were corrected for the finite tunnel effects of solid blockage and the presence of walls as outlined in Barlow et al. (Barlow et al., 1999). Solid blockage is caused by the local water tunnel cross-sectional area being decreased in the vicinity of the model, which by incompressible mass continuity means that the mean local flow velocity must increase. The walls of the tunnel produce upwash on the model, which changes the effective α. For all models tested, the maximum decrease in C_L due to finite tunnel effects was 0.0693, the maximum increase in C_D was 0.0637 and the maximum increase in α was 1.57 deg.

The trend for the highest mean maximum lift coefficient ($C_{L,max}$) was consistent for all trials, with the medium swim speed group

Table 3. Mean (± one s.d.) values for animal swim speed groups and hydrodynamic parameters

Swim speed group	$C_{L,max}$	$\alpha_{C_{L,max}}$ (deg.)	$C_{D,min}$	$\alpha_{C_{D,min}}$ (deg.)
Reynolds number (*Re*) match				
Slow	1.008 (0.140)	24.7 (7.0)	0.041 (0.008)	–2.0 (1.7)
Medium	1.328 (0.124)	31.8 (7.2)	0.027 (0.009)	–5.4 (7.8)
Fast	1.034 (0.117)	39.0 (6.1)	0.029 (0.013)	0.3 (7.1)
$2\,m\,s^{-1}$ swim speed match				
Slow	0.985 (0.195)	24.0 (7.0)	0.038 (0.005)	–1.7 (1.5)
Medium	1.287 (0.090)	31.2 (7.2)	0.047 (0.021)	–4.2 (6.1)
Fast	1.064 (0.066)	39.7 (7.2)	0.028 (0.010)	2.0 (9.8)

Slow swim speed group: *Inia geoffrensis* and *Kogia breviceps*; medium swim speed group: *Tursiops truncatus* and *Phocoena phocoena*; fast swim speed group: *Delphinus delphis*, *Lagenorhynchus acutus*, and *Stenella coeruleoalba*. $C_{L,max}$, maximum lift coefficient; $\alpha_{C_{L,max}}$, angle of attack at maximum lift coefficient; $C_{D,min}$, minimum drag coefficient; $\alpha_{C_{D,min}}$, angle of attack at minimum drag coefficient; *Re*, Reynolds number.

having the highest mean $C_{L,max}$ followed by the fast group and the slow group (Table 3). The mean $C_{L,max}$ for the medium swim speed group was 32% higher than the slow group and 28% higher than the fast group for the *Re* match trials. For the $2\,m\,s^{-1}$ swim speed match trials, the mean $C_{L,max}$ for the medium swim speed group was 31% higher than the slow group and 21% higher than the fast group. The trend for highest mean angle of attack at the maximum lift coefficient ($\alpha_{C_{L,max}}$) was also consistent for both the *Re* and swim speed match trials but different than that for highest mean $C_{L,max}$, with the fast swim speed group having the highest mean $\alpha_{C_{L,max}}$, followed by the medium swim speed group and the slow swim speed group. This indicated that the animals in the fast swim speed group had flippers that were the most successful in delaying stall. $C_{L,max}$ for the fast swim speed group occurred at α that was 14.3 deg. greater than the slow swim speed group and 7.2 deg. greater than the medium swim speed group for the *Re* match trials, and was 15.7 deg. greater than the slow swim speed group and 8.5 deg. greater than the medium swim speed group for the $2\,m\,s^{-1}$ swim speed match trials.

The mean minimum drag coefficient ($C_{D,min}$) occurred at negative angles for the slow and medium swim speed groups, and occurred at a positive angle for the fast swim speed group (Table 3). The lowest $C_{D,min}$ for *Re* and swim speed matching was found for the medium and fast swim speed groups, respectively. The mean $C_{D,min}$ for the medium swim speed group for the *Re* match trials was 34% lower than the slow swim speed group and 7% lower than the fast swim speed group. For the $2\,m\,s^{-1}$ swim speed match trials, the mean $C_{D,min}$ for the fast swim speed group was 26% lower than the slow swim speed group and 40% lower than the medium swim speed group.

In general, all of the hydrodynamic parameters did not significantly vary between the *Re* match and $2\,m\,s^{-1}$ swim speed match trials. The major exception to this was the mean $C_{D,min}$ for the medium swim speed group, which increased by 74% from the *Re* match trials to the $2\,m\,s^{-1}$ swim speed match trials.

All C_L *versus* α curves for *Re* of 250,000 could be grouped according to whether their behavior was linear or nonlinear in the non-stall region (Figs 3 and 4; Table 1). It was found that planform shape was directly related to whether or not the curve of C_L was linear in the non-stall region, so the results presented in the current study are differentiated by whether or not their lift curves are linear. An engineered hydrofoil with linear behavior in the non-stall region was also tested by the authors in the water tunnel (*Re*=200,000) and its C_L *versus* α curve is additionally presented in Fig. 3 for comparison. The C_L *versus* α curve for an engineered swept wing (Murray et al., 2005), exhibiting nonlinear behavior in the non-stall region is additionally presented in Fig. 4 for comparison with the cetacean curves. All models tested had C_D *versus* α curves that were qualitatively the same, demonstrating a parabolic shape in the non-stall region (Fig. 5). The C_D *versus* α curve for an engineered hydrofoil tested by the authors in the water tunnel is additionally presented in Fig. 5 for comparison with the cetaceans.

For tests in which the swim speed was $2\,m\,s^{-1}$, all values of C_L *versus* α curves could also be grouped according to linear or nonlinear behavior in the non-stall region (Figs 6 and 7). No models changed categories (i.e. the models that had nonlinear lift curves for the *Re* match trials also had nonlinear lift curves for the $2\,m\,s^{-1}$ match trials and *vice versa*). C_D *versus* α curves showed that all of the drag curves were qualitatively the same with a parabolic shape in the non-stall region (Fig. 8). Table 2 shows various hydrodynamic properties of interest for these $2\,m\,s^{-1}$ swim speed match trials to include the flipper (and therefore animal) *Re* at the $2\,m\,s^{-1}$ testing speed. The flipper *Re* varied from a minimum of 118,000 (*K. breviceps* 059) to a maximum of 374,000 (*D. delphis* 070).

DISCUSSION

Previously reported data on the hydrodynamic performance of the flippers were from the examination of the flippers of baleen whales (Suborder Mysticeti, Family Balaenopteridae), including individual analysis of the humpback whale and minke whale (Miklosovic et al., 2004; Cooper et al., 2008). The present study is the first comparative examination of the hydrodynamic lift and drag characteristics of odontocete (Suborder Odontoceti) cetacean flippers, focusing on animals in the families Delphinidae (*D. delphis, L. acutus, S. coeruleoalba, T. truncatus*), Iniidae (*I. geoffrensis*), Kogiidae (*K. breviceps*) and Phocoenidae (*P. phocoena*). As opposed to the flippers of the balaenopterids, the flippers of these species have restricted mobility (Howell, 1930; Fish, 2004). As a result, the flippers cannot be appressed against

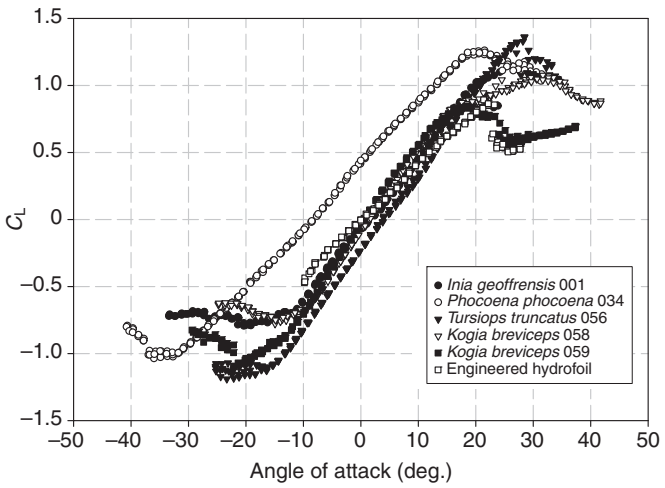

Fig. 3. Lift coefficient (C_L) *versus* angle of attack (α), Reynolds number=250,000 match trials. Only the curves that are linear in the non-stall region are shown. The C_L *versus* α curve for an engineered hydrofoil is shown for comparison.

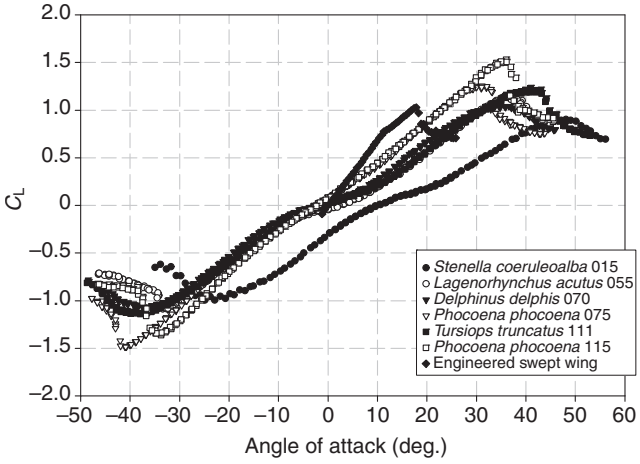

Fig. 4. Lift coefficient (C_L) *versus* angle of attack (α), Reynolds number=250,000 match trials. Only the curves that are nonlinear in the non-stall region are shown. A C_L *versus* α curve for an engineered swept wing, which also exhibits nonlinear behavior in the non-stall region is presented for comparison.

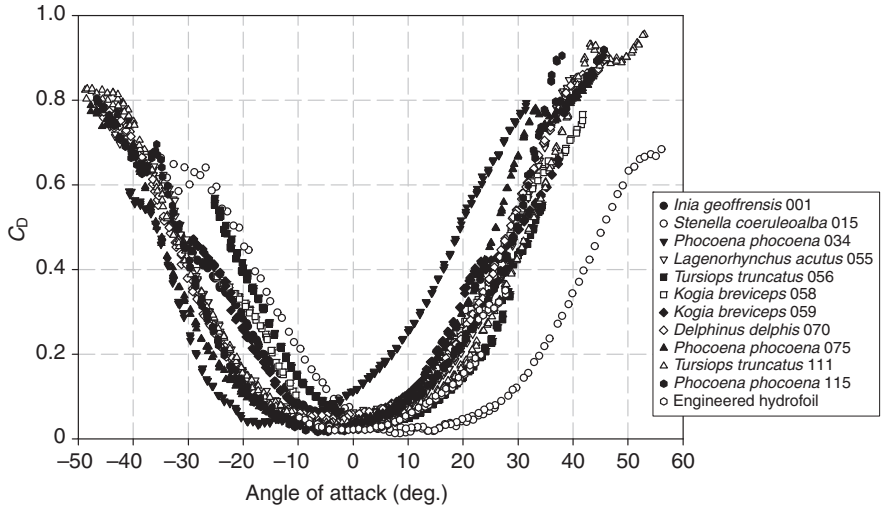

Fig. 5. Drag coefficient (C_D) *versus* angle of attack (α), Reynolds number=250,000 match trials. All cetacean flipper models displayed the same qualitative drag behavior consisting of parabolic curves in the non-stall region. The C_D *versus* α curve for an engineered hydrofoil is also presented for comparison.

the body and always present a wing-like structure to the flow. Furthermore, movements of the flippers can change the sweep angle and the hydrodynamic performance of the flippers. Thus, the combined lift and drag performance is important at all times to these cetaceans.

Due to experimental limitations, the flippers were not tested at an α of 90 deg., so the performance of the flippers for braking could not be assessed. With the flow normal to the flipper surface, drag would be the dominant force imposed on the flipper. Under such conditions, flippers with high aspect ratios (AR=span^2/planform area) would have higher C_D than compared with low AR flippers (Hoerner, 1965). A high AR indicates a long narrow geometry whereas a low AR indicates a broad area with a short span (Webb, 1975; Vogel, 1994). Ultimately, braking force would be associated with interaction the C_D and planform area of the flipper.

The odontocetes examined in the present study exhibit considerable variation in habitat, swimming speed and maneuverability (Fish and Rohr, 1999; Fish, 2002). *Inia* is a slow but highly maneuverable swimmer that moves through rivers and flooded forests. Routine swimming speeds for *Inia* are 0.4–0.9 m s^{-1} (Best and da Silva, 1989). *Lagenorhynchus*, *Stenella* and *Delphinus* are found in the pelagic off-shore environment and are fast swimmers with routine swimming speeds of 1.7–5.8 m s^{-1} and maximum speeds of 7.7–13.9 m s^{-1} (Fish and Rohr, 1999). *Lagenorhynchus* can turn at high rates but with a relatively large turning radius (Fish, 2002). *Tursiops* swims and maneuvers at lower rates. *Tursiops* is found in both off-shore and in-shore habitats, where this species can inhabit shallow bays and estuaries. Similarly, *Phocoena* is coastal and inhabits restricted bays and harbors. *Phocoena* swims at 1.3–2.8 m s^{-1} (Bel'kovich, 1991; Curren et al., 1994). Relatively little is known about the habits of *Kogia*, although it exhibits slow movements with a routine swimming speed of 1.5 m s^{-1} (Morzer and Brown, 1971) and resides off the continental shelf.

The C_L and C_D *versus* α curves for all the species examined were similar in shape to those of typical modern engineered hydrofoils or airfoils (Figs 3–5 present plots of curves for engineered foils in addition to those of the cetacean curves). As the flipper models were exact replicas of the geometry found in nature, which tended to be non-symmetrical with variable surface geometry, the curves are not as smooth and symmetrical as expected for a modern engineered foil (Abbott and von Doenhoff, 1959). This non-symmetry also meant that the cross-sectional profile along the flipper model was

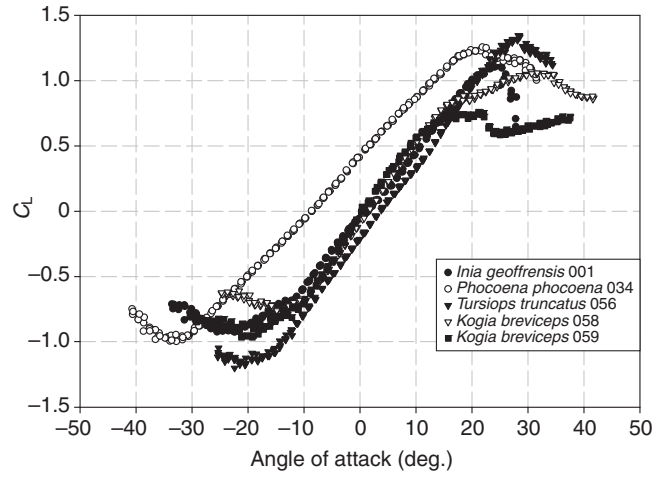

Fig. 6. Lift coefficient (C_L) *versus* angle of attack (α), swim speed=2 m s^{-1} match trials. Only the curves that are linear in the non-stall region are shown.

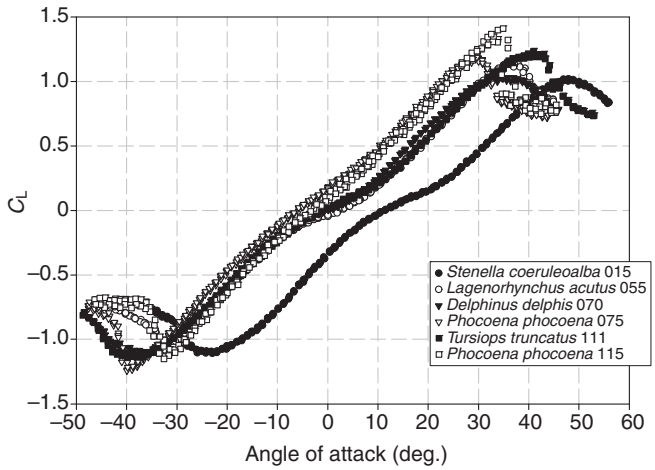

Fig. 7. Lift coefficient (C_L) *versus* angle of attack (α), swim speed=2 m s^{-1} match trials. Only the curves that are nonlinear in the non-stall region are shown.

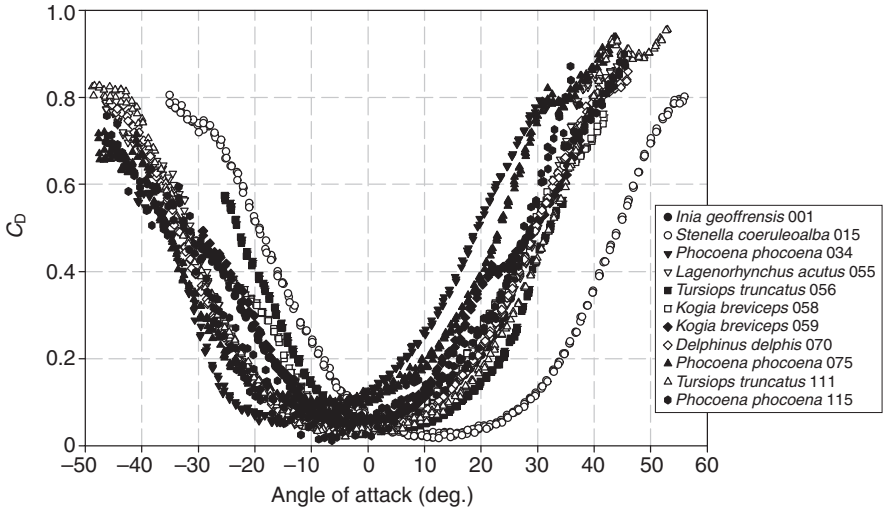

Fig. 8. Drag coefficient (C_D) *versus* angle of attack (α), swim speed=2 m s^{-1} match trials. All cetacean flipper models had parabolic drag curves in the non-stall region (i.e. were qualitatively similar).

not constant. Values such as camber and thickness-to-chord ratio were not constant for these flippers, although these values are constant for many ideal and manufactured hydrofoils. This difference meant that means had to be considered.

Even though the flippers were non-symmetrical, some generalizations from wing theory may still be applied. The C_L *versus* α data (Figs 3, 4, 6 and 7) give a general idea of the camber of the flippers, because the α of zero lift is largely determined by the camber for a hydrofoil (Abbott and von Doenhoff, 1959). A flipper with a positive camber is defined as one that produces a positive value of lift at zero α (and therefore the α of zero lift is negative) and *vice versa*. The most positively cambered flipper was the harbor porpoise (*P. phocoena* 034), and the most negatively cambered flipper was the striped dolphin (*S. coeruleoalba* 015).

The C_D *versus* α curves for the flipper models were found to be qualitatively similar in shape to those of modern hydrofoils, although there are of course quantitative differences as modern hydrofoils are usually designed to minimize drag. However, $C_{D,min}$ of the odontcetes studied was similar to the values previously reported for mysticete flippers (Miklosovic et al., 2004; Cooper et al., 2008). Prior to stall of the odontcete flippers, the C_D displays a common parabolic shape for all model planforms and testing speeds, with each flipper having a unique value of $C_{D,min}$, which is listed in Tables 1 and 2. The value of $C_{D,min}$ is only slightly to moderately affected by thickness and camber whereas boundary layer effects and *Re* are the main parameters that determine $C_{D,min}$ (Abbott and von Doenhoff, 1959). The α at the $C_{D,min}$ ($\alpha_{C_{D,min}}$ in Tables 1 and 2) was also found to be unique for each model. A constant relation between the sign (positive/negative) of the camber and the sign of $\alpha_{C_{D,min}}$ was not found.

The C_L *versus* α curves were also found to be qualitatively similar in shape to those of modern hydrofoils. All flipper models exhibited stall characteristics, where a $C_{L,max}$ was obtained and then flow separation and large regions of reversed flow caused a loss of lift as the α was further increased (Tables 1 and 2). The α at the onset of stall (denoted as $\alpha_{C_{L,max}}$ in Tables 1 and 2) was unique for each flipper and varied widely from 18–46 deg. These values exceeded angles measured for mysticete flippers with stall angles for the humpback whale of 16.3 deg. (Miklosovic et al., 2004) and the minke whale of 10–14 deg. (Cooper et al., 2008). Stall for odontocetes tended to be gradual (i.e. the lift curve was smooth as opposed to sharply dropping off) with the exception of the harbor porpoise *P. phocoena* 115 where stall resulted in a sudden loss of lift. There was no qualitative difference between the lift curves for the *Re*=250,000 match trials and the swim speed=2 m s^{-1} match trials, although there were quantitative differences (Tables 1 and 2).

The planform shape of the flippers was found to have a qualitative relation to the shape of the C_L *versus* α curve. For flippers with planforms that were triangular (Table 1), C_L increased linearly with α in the non-stall region (Figs 3 and 6). However, for flippers with planforms that were similar to swept wings (Table 1), C_L showed a nonlinear increase in the non-stall region, although the curves could be characterized as being piecewise linear in the non-stall region, with two distinct slopes present (Figs 4 and 7).

The nonlinear nature of C_L is caused by two different lift generation mechanisms dominating at different α. To visualize this phenomenon, the finite volume computational fluid dynamics (CFD) code COSMOS FloWorks (a package integrated with SolidWorks 2007, Dassault Systèmes SolidWorks Corp.) was used to simulate the flow field around the flipper for *L. acutus* 055, which exhibits a piecewise linear lift curve. FloWorks solves the Reynolds Averaged Navier–Stokes (RANS) equations on a rectangular computational mesh, using the k–ε turbulence model to close the governing fluid flow equations (Figs 9–11). Grid size for the simulation was approximately 800,000 cells. A convergence study was performed, and as the grid size was increased the lift and drag curves converged in the proper direction (i.e. towards the experimental values), which is trademark of a well-defined CFD simulation. The results presented in the current study represent the limit of machine memory (3 GB RAM); if the mesh size was increased further (i.e. a machine with more memory was used) then the predicted results would eventually converge to a grid-independent solution, where subsequent increases in the mesh do not affect the numerical solution (Anderson, 1995).

For the smaller lift curve slope value of 0.0198 deg^{-1}, which occurs at small α, the flow around the flipper is smooth (Fig. 9). This is a region of non-vortex dominated lift, also called potential flow lift. To give a quantitative comparison, an elliptical planform (which is the 'best case' of potential flow lift) of the same aspect ratio as the flipper would have a lift curve slope of 0.0230 deg.$^{-1}$. For larger values of α, the slope of the lift curve becomes steeper (0.0370–0.0397 deg.$^{-1}$) and the flow around the flipper exhibits the presence of vortices (Fig. 10). The results for the high negative α portion of the lift curve (–4 deg. to $C_{L,min}$) are not shown in Fig. 10 but are qualitatively similar to those for the high positive α. The regions of increased lift curve slope are the vortex-dominated lift

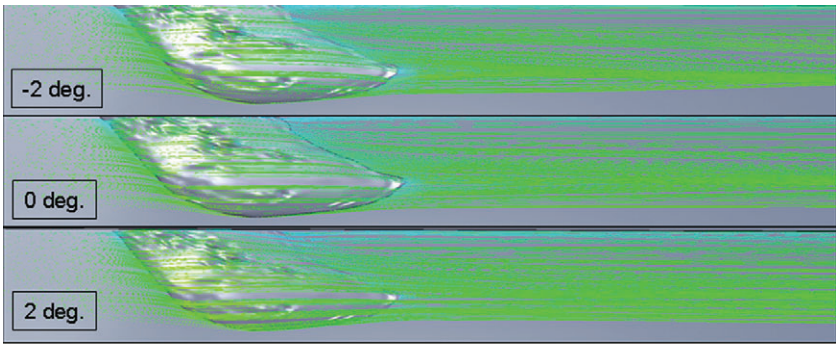

Fig. 9. Computational fluid dynamics visualization of the flow pattern around flipper model for the Atlantic white-sided dolphin (*Lagenorhynchus acutus* 055) showing the pathlines for potential (non-vortex dominated) lift at Reynolds number (*Re*)=250,000. This potential lift mechanism is similar to the lift generation mechanism on non-swept or moderately swept wings. Note that the fluid flows smoothly over the flipper in generally straight lines. The highlighted portion of the lift curve shows the region where this potential lift mechanism applies.

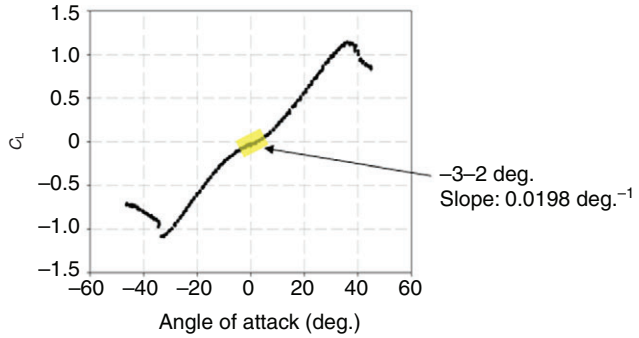

regions, characterized by the increased lift the (stable) vortex produces. Aeroplanes with delta wing planforms exhibit this vortex-dominated lift phenomenon (Hurt, 1965). The vortex increases lift by injecting additional downward momentum into the wake and by the suction peaks associated with the vortex at the leading edge of the wing (Hoerner and Borst, 1985). The low pressures generated by these stable vortices also help contribute to the lift (Houghton and Carpenter, 2003). The lateral flow on the surface of the flipper is caused by fluid being entrained into the vortex core (Fig. 10), which is characteristic of delta wings producing vortex-dominated lift. As expected, the resultant lift curve slopes in the vortex-dominated lift regions are greater than the theoretical elliptical planform lift curve slope. In fact, the total lift in the vortex-dominated lift region may be viewed as a result of the sum of the potential lift and the vortex-dominated lift (Hoerner and Borst, 1985).

Vortex-dominated lift implies that the vortex is a major factor in the lift generation. Wings that operate on potential lift, such as rectangular wings, still have wing-tip and trailing vortices (Anderson, 2001); very slight tip vortices may be observed in Fig. 9. These vortices in potential flow lift do not play as significant a role in the lift generation. Also, in potential flow the entrainment of fluid into the tip vortex is localized at the wing (flipper) tip itself, whereas in vortex-dominated flow fluid across a large portion of the wing (flipper) leading edge is entrained into the vortex.

Fig. 11 shows a comparison of the experimental and CFD results for C_L *versus* α and C_D *versus* α curves. The question of whether or not the numerically calculated values may be used with confidence is best answered by comparing the simulation results with a known answer (the experimental values in this case), as in Fig. 11. The lift curve simulation results are seen to be in excellent agreement with the experiment in the non-stall region. The CFD simulation accurately predicts the nonlinear behavior of the lift curve. For α near stall and post-stall, the CFD simulation is seen to under-predict the lift. This result is not surprising as the flow field becomes complex in the near-stall and post-stall regions. Large regions of flow separation on the flipper and complex wake behavior occur, which are difficult to predict numerically. However, even though the numerical values of C_L are below the experimental values, the shape of the lift curve predicted numerically is still qualitatively correct.

The numerically predicted values of C_D are generally under-predicted when compared with the experimental data (Fig. 11). However, as with the lift curve, the predicted drag curve is qualitatively similar to the drag data. The main reason for the under-prediction of the drag curve lies with the turbulence model. For the flows present in this experiment, the drag is a result of the pressure distribution over the body (pressure drag and induced drag) and the shear stress distribution over the body (friction drag, caused by the fluid viscosity) (Hoerner, 1965; Anderson, 2001). The friction drag is intimately related to the boundary layer. For the turbulent flows considered in the present study, the fluid velocity field varies significantly and irregularly in both time and position (Pope, 2000), and interactions between the fluid and solid boundary (and thus the boundary layer) are complex. The turbulence model attempts to characterize this three-dimensional irregular flow velocity behavior along with the boundary layer and thus predicting accurate drag values is much more difficult. Other models for predicting turbulence such as the k–ε and Reynolds Stress models do exist (Pope, 2000; Chung, 2002). However, at the time of publication the k–ω model was the only one offered by COSMOS FloWorks and thus comparisons between turbulence models could not be made.

The maximum hydrodynamic efficiency, defined as $(C_L/C_D)_{max}$, was found to be the best for the flipper model of the bottlenose dolphin (*T. truncatus* 056), having a value of 7.567 for the $2\,m\,s^{-1}$ speed match trials and 7.897 for the *Re* match trials. The physical significance of the efficiency is that it represents a measure of the lift that is generated when drag is overcome; for example, the efficiency of 7.567 means that the flipper is producing 7.567 N of lift for every 1 N of drag that is overcome. The lowest hydrodynamic efficiencies were 2.749 for the harbor porpoise (*P. phocoena* 075) $2\,m\,s^{-1}$ match trial and 2.868 for the Atlantic white-sided dolphin (*L. acutus* 055) *Re* match trial. Therefore, the planform of *T. truncatus* 056 is the most hydrodynamically efficient of the models tested.

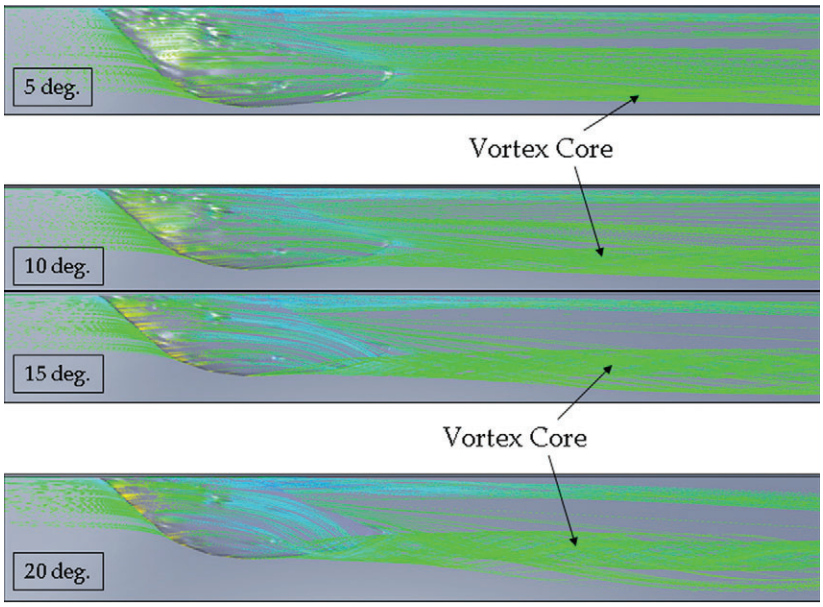

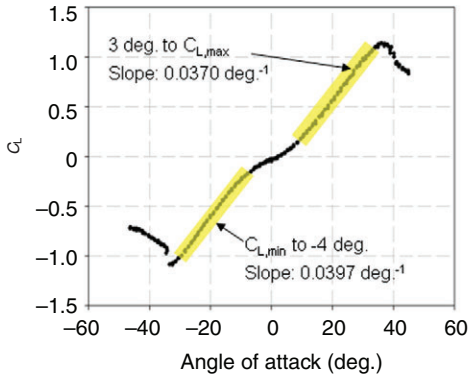

Fig. 10. Computational fluid dynamics visualization of the flow pattern around flipper model for the Atlantic white-sided dolphin (*Lagenorhynchus acutus* 055) showing the pathlines for vortex-dominated lift. The vortex-dominated lift for these Reynolds number (*Re*)=250,000 simulations is created by the presence of a strong vortex that begins along the leading edge of the flipper and strengthens toward the flipper tip. This vortex-dominated lift mechanism is similar to the lift generation mechanism on highly swept or delta wings. Note that as angle of attack increases, an increasing number of the pathlines are rolled into the vortex core and the vortex core gains strength (i.e. is more distinct). The highlighted portions of the lift curve show the regions where this vortex-dominated lift applies.

The hydrodynamic efficiency was greater at 23.2 for the humpback whale (Miklosovic et al., 2004) compared with the odontocete flippers in this study. The humpback whale flipper has a higher AR compared with the flippers of odontocetes in this study. High AR hydrofoils have a high hydrodynamic efficiency. In addition, this high value for hydrodynamic efficiency of the humpback whale flipper may have been exaggerated due to the fact that tests that were performed on an idealized flipper model, which because of its perfectly streamlined cross-section had lower values of C_D than the real flipper models tested in the present study.

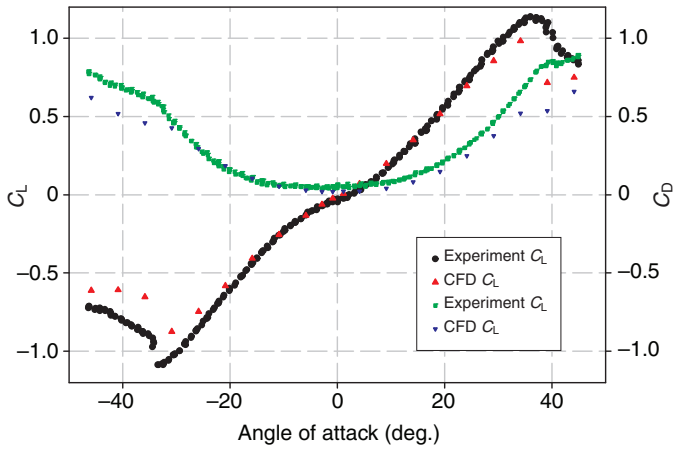

Fig. 11. Experimental *versus* computational fluid dynamics (CFD) results for *Lagenorhynchus acutus* 055. The data in this figure directly correspond to the data used to generate the flow visualizations in Figs 9 and 10. Also note that the nonlinear behavior of the lift curve is predicted by the CFD calculation.

Differences were found in hydrodynamic characteristics ($C_{L,max}$,$C_{D,min}$) of the flippers when the species were sorted in groups based on swimming speed (Table 3). These differences suggest ecological relevance, particularly when size is taken into account (Woodward et al., 2006). Slow swimmers such as *Inia* have relatively broad flippers. This broad flipper would be able to generate a large lift at low speeds despite the low $C_{L,max}$. This combination of low $C_{L,max}$ and relatively large flipper planform area would be effective in swimming in maneuvering at slow speeds in the complex habitats of river systems and flooded forests (Best and da Silva, 1989; Fish, 2002). Conversely, fast swimmers have relatively small flippers for their body size (Fish and Rohr, 1999; Woodward et al., 2006; Cooper et al., 2008). The low $C_{L,max}$ with its concomitant high $\alpha_{C_{L,max}}$ in this case would aid in stability by reducing excessive destabilizing lift forces anterior of the center of mass. As lift increases with the square of the velocity (Eqn 1), a small flipper area and low $C_{L,max}$ would limit torque generation at high swimming speeds and enhance stability. The high value of $C_{L,max}$ for medium speeds swimmers may then represent a compromise between stability and maneuverability at moderate speeds (Fish, 2002).

For $C_{D,min}$, the high values for the 2 m s^{-1} swim speed match of slow and medium speed swimmers may have no serious effect on

flipper drag as, like lift, drag increases with the velocity squared (Eqn 1). Slow and medium speed swimmers will often stop swimming and rest or mill around. *Inia* has been reported to remain stationary and sleep (Best and da Silva, 1989). While spending 45–67% of their time traveling, lower speed activities (i.e. feeding, playing, socializing, resting) occupy the remainder of the daily activity routines of *Tursiops* (Reynolds et al., 2000). For fast swimmers, a low $C_{D,min}$ and relatively small flipper area would help to minimize drag particularly during steady cruising and high-speed sprints (Fish and Rohr, 1999).

There was some variation in hydrodynamic parameters among animals of the same species observed in this work (Tables 1 and 2). Although this result was not the primary focus of this study, there are some preliminary points to be made here to explain this variation. The main explanation for this phenomenon is that all of these models were created from CT scans of real animal specimens. No two animal specimens of the same species and therefore no two models were exactly the same. Individual variation, post mortem effects and preservation could affect the geometry of each flipper. Therefore, some variation in the hydrodynamic characteristics within a species was to be expected. Still to be addressed are changes in flipper geometry associated with age. Studying ontogenetic changes while controlling individual variation requires the examination of known animals from birth to adulthood. The success of captive breeding programs for dolphins may allow us to track the changes of flipper shape with age in the future.

In summary, we found that cetacean flippers exhibit lift and drag curves that are similar to those of modern hydrofoil control surfaces found on engineered devices. The results reported in this work include $C_{L,max}$ and $C_{D,min}$, the α at which the maximum lift and minimum drag occur and lift curve slope(s) for specimens from seven odontocete cetaceans. An unanticipated finding of this work was the unique nonlinear lift curve behavior of flippers with swept-wing-like planforms caused by the onset of vortex-dominated lift. Ecology, morphology and performance requirements are all factors that influenced the evolution of cetacean flippers, and these factors are all linked to the resultant hydrodynamic characteristics of the flippers. Our future research will aim to establish this link more clearly.

LIST OF ABBREVIATIONS

A	planform area (m^2)
AR	aspect ratio
$\bar{C}$	mean aerodynamic chord (m)
C_D	drag coefficient
$C_{D,min}$	minimum drag coefficient
CFD	computational fluid dynamic
C_L	lift coefficient
$C_{L,max}$	maximum lift coefficient
$(C_L/C_D)_{max}$	maximum hydrodynamic efficiency
CT	computed tomography
$F_{L,D}$	lift/drag force (N)
Re	Reynolds number
U	freestream flow velocity ($m\,s^{-1}$)
v	kinematic viscosity
α	angle of attack (deg.)
$\alpha_{C_{D,min}}$	angle of attack at the minimum drag coefficient
$\alpha_{C_{L,max}}$	angle of attack at the maximum lift coefficient
ρ	fluid density ($kg\,m^{-3}$)

This work was supported by the National Science Foundation to F.E.F. (principal investigator), L.E.H. and M.M.M., and the technical support staff of the United States Naval Academy. The authors additionally would like to thank the New Bolton Center of the University of Pennsylvania Veterinary School, the New Jersey Marine Mammal Stranding Center, the Natural History Museum of the Smithsonian Institution, the Woods Hole Oceanographic Institution, and specially Julie Arruda, Scott Cramer, Bruno Frohlich, Perry Habecker, Darlene Ketten, Carly Ginter, James Mead, Jana Parson, Charles Potter, Robert Schoelkopf, and Beth Schuelkens for contributions to this work. P.W.W. was supported by the National Defense Science and Engineering Graduate (NDSEG) Fellowship.

REFERENCES

Abbott, I. H. and von Doenhoff, A. E. (1959). *Theory of Wing Sections*, pp. 1-30; 124-187. New York: Dover Publications.
Anderson, J. D. (1995). *Computational Fluid Dynamics: The Basics with Applications*, pp. 322-325. New York: McGraw-Hill.
Anderson, J. D. (2001). *Fundamentals of Aerodynamics*, pp. 15-28; 44-47. Boston, MA: McGraw-Hill.
Barlow, J. B., Rae, W. H. and Pope, A. (1999). *Low-speed Wind Tunnel Testing*, 3rd edn, pp. 367-425. New York: John Wiley.
Bel'kovich, V. M. (1991). Herd structure, hunting, and play: bottlenose dolphins in the Black Sea. In *Dolphin Societies: Discoveries and Puzzles* (ed. K. Pryor and K. Norris), pp. 17-77. Berkeley, CA: University of California Press.
Best, R. C. and da Silva, V. M. F. (1989). Amazon river dolphin, boto *Inia geoffrensis* (de Blainville, 1817). In *Handbook of Marine Mammals Volume 4: River Dolphins and the Larger Toothed Whales* (ed. S. H. Ridgeway and R. Harrison), pp. 1-23. London: Academic Press.
Chung, T. J. (2002). *Computational Fluid Dynamics*, pp. 683-721. Cambridge: Cambridge University Press.
Cooper, L. N., Sedano, N., Johannson, S., May, B., Brown, J., Holliday, C., Kot, W. and Fish, F. E. (2008). Hydrodynamic performance of the minke whale (*Balaenoptera acutorostrata*) flipper. *J. Exp. Biol.* **211**, 1859-1867.
Curren, K. C., Bose, N. and Lien, J. (1993). Morphological variation in the harbour porpoise (*Phocoena phocoena*). *Can. J. Zool.* **71**, 1067-1070.
Fish, F. E. (2000). Biomechanics and energetics in aquatic and semiaquatic mammals: platypus to whale. *Physiol. Biochem. Zool.* **73**, 683-698.
Fish, F. E. (2002). Balancing requirements for stability and maneuverability in cetaceans. *Integr. Comp. Biol.* **42**, 85-93.
Fish, F. E. (2004). Structure and mechanics of nonpiscine control surfaces. *IEEE J. Oceanic Eng.* **29**, 605-621.
Fish, F. E. and Battle, J. M. (1995). Hydrodynamic design of the humpback whale flipper. *J. Morphol.* **225**, 51-60.
Fish, F. E. and Lauder, G. V. (2006). Passive and active flow control by swimming fishes and mammals. *Annu. Rev. Fluid Mech.* **38**, 193-224.
Fish, F. E. and Rohr, J. (1999). Review of dolphin hydrodynamics and swimming performance. In *SPAWARS System Center Technical Report 1801* San Diego, CA.
Fish, F. E., Beneski, J. T. and Ketten, D. R. (2007). Examination of the three-dimensional geometry of cetacean flukes using computed tomography scans: hydrodynamic implications. *Anat. Rec.* **290**, 614-623.
Fox, R. W. and McDonald, A. T. (1999). *Introduction to Fluid Mechanics*, 5th edn, pp. 732-738. New York: John Wiley.
Hoerner, S. F. (1965). *Fluid-Dynamic Drag*. Chap. 2, pp. 1-16, chap. 3, pp. 1-28. Bakersfield, CA: Published by Author.
Hoerner, S. F. and Borst, H. V. (1985). *Fluid-Dynamic Lift*, 2nd edn, chap. 18, pp. 1-20. Bakersfield, CA: Published by Author.
Houghton, E. L. and Carpenter, P. W. (2003). *Aerodynamics for Engineering Students*, 5th edn, pp. 257-269. Burlington, MA: Elsevier Butterworth-Heinemann.
Howell, A. B. (1930). *Aquatic Mammals*, pp. 206-267. Springfield, IL: Charles C. Thomas.
Hurt, H. H., Jr (1965). *Aerodynamics for Naval Aviators*. Norfolk, VA: The Office of the Chief of Naval Operations Aviation Training Division, U.S. Navy.
Johari, H., Henoch, C., Custodio, D. and Levshin, A. (2007). Effects of leading edge protuberances on airfoil performance. *AIAA J.* **45**, 2634.
Marino, L., Uhen, M. D., Pyenson, N. D. and Frohlich, B. (2003). Reconstructing cetacean brain evolution using computed tomography. *Anat. Rec.* **272B**, 107-117.
Miklosovic, D. S., Murray, M. M., Howle, L. E. and Fish, F. E. (2004). Leading-edge tubercles delay stall on humpback whale (*Megaptera novaeangliae*) flippers. *Phys. Fluids* **16**, L39-L42.
Mörzer Bruyns, W. F. J. (1971). *Field Guide to Whales and Dolphins*, pp. 1-258. Amsterdam: Uitgeverij Mees.
Murray, M. M., Miklosovic, D. A., Fish, F. E. and Howle, L. E. (2005). Effects of leading edge tubercles on a representative whale flipper model at various sweep angles. Durham, NH: Conference Proceedings of the 14th International Symposium on Unmanned Untethered Submersible Technology.
Pope, S. B. (2000). *Turbulent Flows*, pp. 3-9; 335-458. Cambridge: Cambridge University Press.
Reynolds, J. E., 3rd, Wells, R. S. and Eide, S. D. (2000). *Bottlenose Dolphin: Biology and Conservation*. Gainesville, FL: University Press of Florida.
Schultz, M. P. and Flack, K. A. (2003). Turbulent boundary layers over surfaces smoothed by sanding. *J. Fluid Eng.* **125**, 863-870.
Shaughnessy, E. J., Katz, I. M. and Schaffer, J. P. (2005). *Introduction to Fluid Mechanics*, pp. 534-563. New York: Oxford University Press.
Thewissen, J. G. M. (1998). *The Emergence of Whales,* pp. 303-324. New York: Plenum Press.
Vogel, S. (1994). *Life in Moving Fluids*. Princeton, NJ: Princeton University Press.
Webb, P. W. (1975). Hydrodynamics and energetics of fish propulsion. *Bull. Fish. Res. Bd. Can.* **190**, 1-158.
Weber, P. W. (2008). Hydrodynamic characteristics of marine animal control surfaces. Master's Thesis, Duke University, Durham, NC, USA.
Woodward, B. L., Winn, J. P. and Fish, F. E. (2006). Morphological specializations of baleen whales associated with hydrodynamic performance and ecological niche. *J. Morphol.* **267**, 1284-1294.